Applied Nanoscience (2021) 11:1411–1425
https://doi.org/10.1007/s13204-021-01743-5

ORIGINAL ARTICLE

Bioproduction of CuO and Ag/CuO heterogeneous photocatalysis-photocatalytic dye degradation and biological activities

C. Parvathiraja[1] · S. Shailajha[1]

Received: 7 January 2021 / Accepted: 12 February 2021 / Published online: 27 February 2021

Abstract
Water contamination is a critical and severe issue all over the world. The nano-based particles have the potency to overcome water contamination. In the present work, CuO and Ag/CuO nanoparticles (NPs) were synthesized by *Cyperus pangorei* extract using the co-precipitation method. The plant extract acts as a reducing and stabilizing agent. The purpose of plant extract is to reduce the negative impact of the synthesis method and its derivatives. The Ag^+ and Cu^+ reduction were confirmed through the surface plasmon resonance in the DRS spectrum. The bandgap decreasing is informed that the results have opted in the optical and catalytical applications. CuO bandgap is higher than the Ag/CuO NPs ($\Delta Eg = 0.55$ eV) reveals the Ag/CuO NPs have remarkable optical and catalytic applications. The NPs crystalline nature and size were analyzed by XRD. SEM and TEM analyses characterized the morphology and size variation of the CuO and Ag/CuO NPs. The EDX analysis analyzed the composition of the elements in the synthesized NPs. The FTIR analysis was performed to confirm the possible functional groups of plant extract involved in chemical reduction and bondings. Copper and silver metals and oxygen valencies and binding energies were examined by XPS. Occasionally, contagious diseases shake the world and affected human healthiness because of their pathogenic activity. Mostly, they are resolved by nanoparticles. The biosynthesized CuO and Ag/CuO NPs were performed against Gram-positive (*Staphylococcus aureus—S. aureus*) and Gram-negative (*Escherichia coli—E. coli*) bacteria. The results showed better activity in *E. coli* compared to *S. aureus* in both CuO and Ag/CuO NPs. The photocatalytic activity of CuO and Ag/CuO NPs were analyzed against Rhodamine B (Rh-B) dye under visible light irradiation. The metallic Ag-doped with CuO NPs improves the catalytic compared to pure CuO NPs. The pseudo-first-order kinetics were found to increase the rate of dye degradation by adding Ag ions to the CuO surface. The advanced oxidation process would increase the electron–hole pair activity and reactive oxygen species (ROS) formation. The AOP photocatalyst is widely used to remove the toxicity of wastewater. There is no secondary product formation and rich activated electrons. The obtained results indicate the CuO and Ag/CuO NPs may further use in wastewater treatment and biomedical applications.

Keywords Biosynthesis · Advanced oxidation process · XRD · TEM · Dye degradation and antibacterial activity

Introduction

The day-to-day life advancement is increasing the products and usage of the water. The rapid increase of industrialization and population mostly affects the environment and creates multiple queries and challenges about the sustainable green ecosystem. Nanoparticles are used to clean and protect the hygienic environment by increasing new technologies in industries. As the nanoparticles in solution, gel, slurry, and powder forms are used in various industries such as cosmetics, sewage cleaning, machining, medical, etc. The nanoparticles discovery increases the products and decreases the workforce in industries, which can promote a large number of products to the companies. The products are also eco-loving in nature due to their formation of nanoparticles (Xie et al. 2020; Zhang et al. 2012a, b, 2013, 2015, 2016, 2017a, b, 2018, 2019, 2020a). Environmental pollution caused water pollution, which leads to all pollutions on the earth. The water has been affected by dyes and toxic organic compounds, and often, the aquatic ecosystem was mostly polluted by dyes (Singh et al.

✉ S. Shailajha
drsshailajha@msuniv.ac.in

[1] Department of Physics, Manonmaniam Sundaranar University, Tirunelveli-12, Tamil Nadu, India

2020; Zou et al. 2020; Wang et al. 2020a; Yan et al. 2020). Hence, researchers are focusing on resolving environmental pollution and remove toxic water contaminants. Therefore, they involve in establishing novel advanced techniques for wastewater treatment. Dye degradation is one of the efficient methods of wastewater treatment. The dye degradation process includes flocculation, adsorption, chlorination, stripping, and filtration (Picos-Corrales et al. 2020; He et al. 2020; Takasuga et al. 2020; Ruan et al. 2020; Zhang et al. 2020b). These techniques are old, high energy consumption, time-consuming, costly, and produce the secondary pollution of solid waste that can affect the environment. These drawbacks can resolve by the advanced oxidation process (AOP). AOP is mostly used in wastewater treatment and biological activity. Different types of AOP processes such as Fenton reaction, electrochemical reaction, supercritical water oxidation, ozone reaction, heterogeneous photocatalysis reaction and H_2O and water air oxidation are available to remove pollutants (Tavares et al. 2020; Wang et al. 2020b; Scandelai et al. 2020; Abrile et al. 2020; Liu et al. 2020; Linke et al. 2020). Among the AOP process, heterogeneous photocatalysis has high potential and stability, low cost to remove the pollutants, organic compounds, and dyes from the wastewater. Metal-doped heterogeneous photocatalysis was proven the best removal of the oxidative process from the wastewater (Kumaravel et al. 2019). The metal coupled oxidative process having a low intensity, molecular weight, and toxicity to the environment. The process increases and alters the charge carriers to energy, which creates high absorption. The formed reactive species is based on the catalytic reaction and oxidative process of the metal ions. Among the metal and metal oxide NPs, copper oxide NPs have high exciton binding energy value, high conductivity, and high thermal conductivity. The optical and electronic activities are suitable compared to the other materials. The copper oxide NPs are widely used in the heterogeneous photocatalytic AOP process due to their redox potential, electron transfer process, and p-type material with a narrow bandgap of 1.85 eV (Bulk). The copper oxide NPs' surface was modified by doping elements such as Au, Mg, Mn, and Ni to enhance the oxidation process (Komeilibirjandi et al. 2020; Masudy-Panah et al. 2017; Raveesha et al. 2019; Parvathiraja et al. 2020; Hariram et al. 2021). Besides the metal-doped with CuO, Ag has good stability and catalytic activity, increasing the surface area and optical activity. Silver NPs are widely used in biological activity because of their strong antimicrobial efficiency (Masudy-Panah et al. 2017; Shafey 2020). Silver combination with metal oxide-induced the catalytic and biological activities due to their size reduction, fast nucleation growth, and interaction with the biological and catalytic compounds (Shafey 2020). Biosynthesized NPs have betterment to the chemical synthesis NPs. These are the high activity of optical, magnetic and catalytic properties and large surface area to absorb the pollutants and non-hazardous activity to the environment. *Cyprus pangorei* plant is predominantly containing cellulose and lignin. Cellulose is the primary compound of the plant extract. Moreover, the cellulose matrix is responsible for the reduction, stabilization, and capping of the metal and metal oxide nanoparticles formation. The reaction of plant compounds with the materials is nature friendly, and the polysaccharides carry out the biochemical reactions. They strongly interface with the chemical materials and donate the electrons to build the metal and metal oxides formation without hindering and making zero-valent atoms (Sharifpour et al. 2019; Baturay et al. 2016; Yu et al. 2017). In this work, we report the biosyntheses of CuO and Ag/CuO NPs using the *Cyperus pangorei* plant extract. Here, the plant extract promotes the reduction process and surface modification with the Ag and CuO. The AOP process of heterogenous photocatalysis in CuO and Ag/CuO was studied in detail. Further, the catalytic and biological activities were examined for CuO and Ag/CuO NPs.

Materials and methods

Materials

Silver nitrate ($AgNO_3$, 99.9% purity), Copper (II) nitrate trihydrate $Cu(NO_3)_2{\cdot}3H_2O$, and Rhodamine B ($C_{28}H_{31}C_lN_2O_3$; 99.9% purity) were purchased from HiMedia, India. The purchased chemicals were obtained in analytical grade and used without further purification. *Cyperus pangorei* plants were collected from Manonmaniam Sundaranar University campus, Tirunelveli District, Tamilnadu, India.

Preparation of plant extract

The leaf of *Cyperus pangorei* plants (15 g fresh leaves) was washed with tap water. The washed leaf was mixed with 100 ml double-distilled water in a round bottom flask. The mixed compounds are heated at 60 °C for 30 min and filtered by Whatman No. 1 filter paper. The obtained solution was stored at 4ºC for further studies.

Biosynthesis of CuO and Ag/CuO NPs

CuO NPs were synthesized from the addition of 10 ml of a plant extract with 1 M $Cu(NO_3)_2{\cdot}3H_2O$ solution. The solution was stirred at constant rpm in a magnetic stirrer. The color change from light green to dark brownish color indicates the formation of CuO NPs. The collected samples were centrifuged three times at 5000 rpm for 10 min and washed with double-distilled water. Finally, the obtained precipitate was filtered by Whatman No. 1 filter paper and kept in an

oven at 100 °C for 1 h. The collected samples were used for further characterization.

Ag/CuO NPs were synthesized by $Cu(NO_3)_2{\cdot}3H_2O$ solution in 1 mol and $AgNO_3$ solution in 0.1 M concentration using 10 ml of plant extract and dissolved in 100 ml double-distilled water at room temperature. The mixed solution was stirred, and the obtained solution color was changed. The color change confirms the zero-valency reduction to the NPs. The resultant solution was centrifuged thrice at 5000 rpm for 10 min using double-distilled water. The collected precipitate was filtered and kept in the oven for 1 h. The obtained powder was stored for further characterization.

Characterization of NPs

Crystalline nature and structural information are derived from Pro Powder X'Celerator diffractometer PANalytical X'Pert with Cu Kα (1.5405 Å) in 30 kV and 40 mA. The functional chemical bonds were identified from FT-IR Perkin Elmer in the wavenumber range 4000–400 cm^{-1}. The optical properties and SPR are observed using UV–Visible DRS (UV-2600 Shimadzu) reference as BaSO4. The surface morphology and nano sizes are collected from SEM (Carl Zeiss) and TEM (Titan), and elemental composition were utilized by EDX. The binding energy and valency of biosynthesized NPs were analyzed using the X-ray photoelectron spectroscopy (XPS, PHI 5000 Versa Probe III, Physical Electronics, USA).

Biological activity

Antibacterial activity

The antibacterial activity of biosynthesized CuO and Ag/CuO NPs were examined using Gram-positive *Staphylococcus aureus* (ATCC 6538) and Gram-negative *Escherichia coli* (ATCC 8739) through the well diffusion method. About 10^{-6} CFU/ml of bacterial culture was inoculated into the nutrient broth and incubated overnight. After incubation, the culture was swabbed on sterilized Petri plates containing Mueller–Hinton agar. The well of about 5 mm diameter was made by gel puncture on agar plates, and separately different concentrations of CuO and Ag/CuO NPs (5, 10, 15, and 20 µg/ml) were poured on agar plates. After that, the plates were incubated at 37 °C for 24 h. After incubation, the activity was measured by zone of inhibition on mm scale.

Optical density measurements

The optical density of CuO and Ag/CuO NPs loaded bacterial culture, and pure bacterial culture was measured at 600 nm. The well-grown bacteria *S. aureus* and *E. coli* were suspended with different concentrations (5, 10, 15, and 20 µg/ml) of CuO and Ag/CuO NPs. The suspended solution was kept in an incubator with continuous shaking for different time intervals up to 120 min. The mixed solution was taken out every 15 min and diluted in 3 ml double-distilled water and monitored the growth of bacteria by measuring the OD value at 600 nm.

Photocatalytic activity

The biosynthesized CuO and Ag/CuO NPs catalytic activity were examined by Rh-B dye solution under visible light irradiation. The initial Rh-B concentration of dye is 30 mg/l. 100 ml dye solution dissolved in 10 mg nanocatalyst (CuO and Ag/CuO) and stirred in dark condition for 60 min to attain the adsorption–desorption equilibrium. The mixed solution was kept in a closed chamber and irradiated by the Xenon lamp. The irradiated samples (3 ml) were taken out at every 30 min time interval for 120 min. Consequently, the collecting samples were centrifuged at 5000 rpm for 10 min to remove the catalyst. Later the samples were filtered and characterized by UV–vis spectroscopy. The rate of dye degradation is analyzed using the below-mentioned formula:

$$\text{Photo - catalytic dye degradation}(\%) = \left(C_o - C_t\right)/C_o \times 100,$$

where the initial dye concentration is C_o (before light irradiation) and the concentration of the dye at different irradiation intervals is C_t (Sharifpour et al. 2019).

Results and discussion

UV–visible DRS analysis

Figure 1a represents the biosynthesized CuO and Ag/CuO NPs' absorption, and bandgap energy was analyzed by the UV–visible diffuse refelctane spectrometer (DRS) technique. The peak of biosynthesized CuO NPs showed a peak in 376 nm to demonstrate the presence of Cu^{2+} ions. The absorption edge was formed through the interaction between the Cu^{2+} and O^{2-} transfer of charges (Rasoulpour and Jafarirad 2017). The Ag/CuO NPs spectrum of absorption was edge at 473 nm due to the SPR effect (Fig. 1a). In the Ag/CuO spectrum, the peaks are shifted to redshift compared to CuO NPs denotes Ag decoration in the Cu^{2+} surface. The transition of charge $Ag^{+}/Cu^{2+} \rightarrow O^{2-}$ increase the optical property (Ranjith et al. 2018). The charge transfer was led by the interaction of the flavonoids, fatty acid, and phenolic compounds into the NPs. The Kubelka–Munk theory was to find the bandgap energy of the NPs (Tunc et al. 2010). The bandgap energy spectrum is shown in Fig. 1b. The bandgap values are 2.11 and 1.56 eV for CuO and Ag/CuO NPs, respectively. The bandgap energy difference is

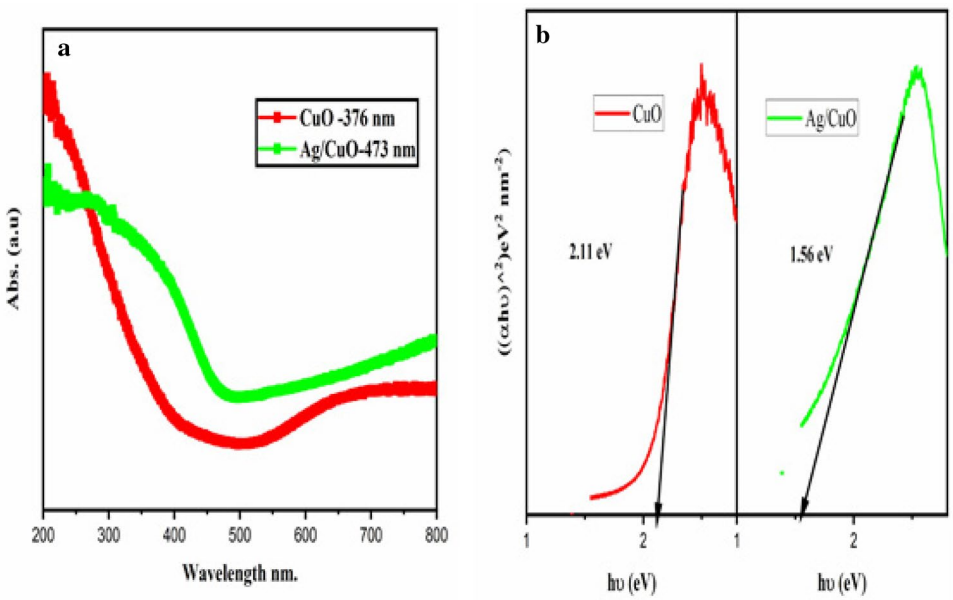

Fig. 1 **a** and **b** DRS spectrum and bandgap energy spectrum of CuO and Ag/CuO NPs

0.55 eV demonstrated in the redshift. The decreasing bandgap energy promotes the active sites of electrons to the holes movement on the CuO surface, and the interaction may increase the oxidation process. The surface plasmon resonance produces the scattering possibility, penetration ability to the radiation and gives the reduction profiles to the surface. These facts are performed and generated the holes and electron separation on the surface, enhancing the oxidation process (Bandara et al. 2005). The valance band and conduction band positions of the CuO and Ag/CuO NPs are evaluated at the zero point charge for the following equation (Wang et al. 2015).

$$E_{VB} = X - \mathrm{Ee} + 0.5\ \mathrm{Eg}, \tag{2}$$

where E_{VB} is the valence band potential, X is the semiconductor electronegativity of CuO (5.81 eV). Ee (4.5 eV) is hydrogen scale-free electron energy and Eg is the bandgap energy of the NPs. In this work, E_{VB} and E_{CB} are 2.365 eV and 0.255 eV for CuO NPs. Similarly, Ag/CuO NPs E_{VB} and E_{CB} are 1.59 eV and 0.03 eV.

FTIR analysis

The Fourier transform infrared (FTIR) study gives information about the purity and surface modification of the NPs. Figure 2 shows the spectrum of biosynthesized CuO and Ag/CuO NPs. The broad and intense peaks of 3100–3500 cm^{-1} are attributed to the OH stretching to the hydrogen bonds on the surface (Kumar et al. 2014). The peak at 2340 cm^{-1} was observed from atmospheric CO_2 (instrument) (Jyoti et al. 2016). 1763 cm^{-1} can be attributed to the aldehyde (carbonyl group) due to the presence

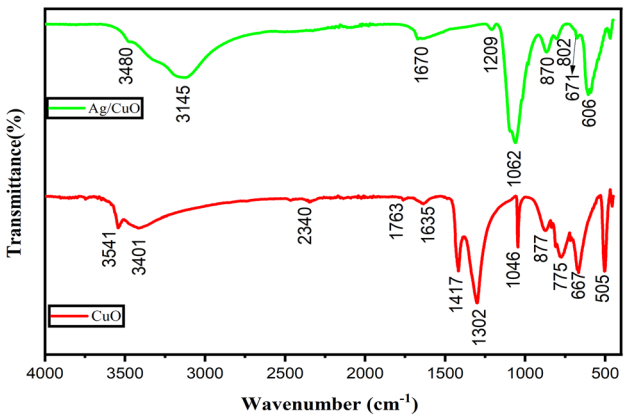

Fig. 2 FTIR spectrum of CuO and Ag/CuO NPs

of phytochemicals from the plant extract. The peaks 1635 and 1670 cm^{-1} correspond to the proteins of amide I bond from the plant extract (Gunalan et al. 2012). The peaks 1062 and 1046 cm^{-1} derived from the carboxylic and phenol groups. The peaks under the 1000 cm^{-1} indicate the presence of metal–oxygen interaction. The peak 775 cm^{-1} confirmed the reduction of nitrate compound in N–H bond vibration from secondary amine (Farmer and Russell 1966). The peaks at 667 and 505 cm^{-1} are characteristics of the Cu and O bond (Sankar et al. 2014). The CuO peak of 877 cm^{-1} shifted to the lower wavelength side at 870 cm^{-1} when adding to silver on the CuO surface. The peaks 606, 678, and 802 cm^{-1} are attributed to the Ag–Cu–O formation by the plant extract. The observed peaks are strongly inferred from the results of reduction and surface addition of Ag and CuO NPs.

XRD analysis

Figure 3 shows the X-ray diffraction (XRD) pattern of biosynthesized CuO and Ag/CuO NPs, which confirm the crystallinity of the NPs. In CuO NPs, peaks are observed at $2\theta = 32.50$, 35.50, 38.70,38.90 46.40, 48.70, 53.50, 58.30, 61.50, 66.20, 68.10, 72.40, and 75.20 which corresponds to (1 10), (0 0 2), (1 1 1), (2 0 0), (1 1 − 2), (2 0 − 2), (0 2 0), (2 0 2), (1 1 − 3), (3 1 − 1), (2 2 0), (3 1 1), and (2 2 − 2) planes of monoclinic structure and good agreement with the standard JCPDS Card No. 48-1548. There are no impurities observed in the spectrum. The plant extract reactions emanate the crystallinity of the CuO NPs. In addition to Ag into CuO surface as shown in the spectrum (Fig. 3). The Ag/CuO NPs peak at $2\theta = 38.70$, 44.30, 64.40, and 77.410 which represent the planes (1 1 1), (2 0 0), (2 2 0), and (3 1 1) and the remaining peaks of CuO NPs. The Ag presence is less compared to CuO because of their activity and concentration. The peak at 38° corresponds to (1 1 1) plane indicated both phases of Ag and CuO NPs. The obtained Ag/CuO peaks are in good accordance with standard JCPDS data. The crystalline sizes were calculated by the Debye Scherrer formula (Farmer and Russell 1966). The sizes are 17.84 and 27.24 nm corresponds to CuO and Ag/CuO, respectively. The increased size leads to the lattice orientation, and crystal growth of the CuO NPs surface was modified by Ag cluster or atoms (Hemmati et al. 2018; Wang et al. 2008).

SEM with EDX analysis

The synthesized CuO and Ag/CuO NPs' morphology, size, and elemental presence was monitored by scanning electron microscope (SEM) with energy dispersive X-ray analysis (EDX) (Fig. 4). The biosynthesized CuO NPs show the quasi-spherical shape and their sizes are 10–40 nm (Fig. 4a). The Ag cluster into the CuO surface, the shapes and sizes were reformed to the lattice arrangement of the NPs. Ag/CuO NPs have a spherical shape with the sizes of 20–35 nm (Fig. 4c). Due to the presence silver ions (Ag^+) which are oriented with the copper oxide (Cu^{2+} and O^{2-}) surface. In Ag/CuO, size modification were occurred by the process of lattice oxygen vacancy filled by Ag^+ and Cu^{2+} ions to the surface (Kowalska et al. 2015).

The biosynthesized CuO and Ag/CuO NPs' elemental composition are shown in Fig. 4b and d. Figure 4b shows the Cu and O composition of CuO NPs, which confirm the presence of Cu and O elements. Figure 4d shows the Ag, Cu, and O elemental composition. The low content of Ag was re-assured by EDX values and spectrum.

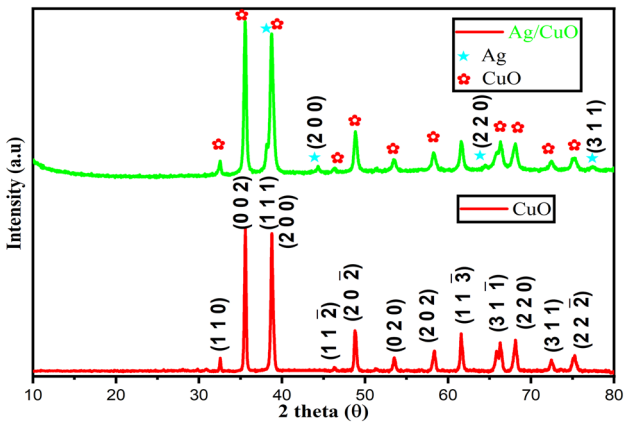

Fig. 3 XRD spectrum of CuO and Ag/CuO NPs

Mapping analysis

The biosynthesized CuO and Ag/CuO NPs atomic arrangement was measured by EDX mapping analysis. Figure 5a and b shows the CuO NPs' mapping, whereas copper and oxygen were spread mutually. Figure 5c–e shows the Ag/CuO NPs' mapping. This combination makes the spectrum of copper richer, when compared to silver and oxygen. Moreover, silver decorated with copper and oxygen atoms are shown in the mapping analysis (Fig. 5c–e).

TEM analysis

The biosynthesized Ag/CuO NPs exhibited the spherical shape images in Transmission Electron Microscopic (TEM) analysis which was depicted in Fig. 6a, b. The size of the Ag/CuO NPs is 17–32 nm, which are nearly closed to the SEM and XRD Ag/CuO sizes. In this work, we used the *Cyperus pangorei* extract, which is responsible for the growth of Ag/CuO NPs. Ag^+ ionic potentials are more robust than the Cu^{2+} ions, while the morphology denotes Ag cluster formation to the CuO surface. The lattice fringes reveal the measurements of 0.26 nm of (2 0 0) plane, 0.23 nm of (1 1 1) plane for CuO and Ag, respectively. Owing to their atomic orientation relationship, they formed the phase of Ag decoration in the surface of CuO, and the values of the lattice fringes are almost closed to the Ag and CuO (Fig. 6c). The electrochemical potential of Ag and Cu were mostly oxidized as Cu atoms.

The plant extract compounds may be reduced and mixed with the Cu_2O nucleate O ions. The phase will change further oxidization by CuO and expand to Cubic forms. The Ag cluster is oriented towards the surface of CuO (Peng et al. 2012). It explores the form of cubic, which is strongly modified to spherical shape. The SAED pattern rings show the polycrystalline nature of the biosynthesized Ag/CuO NPs (Fig. 6d).

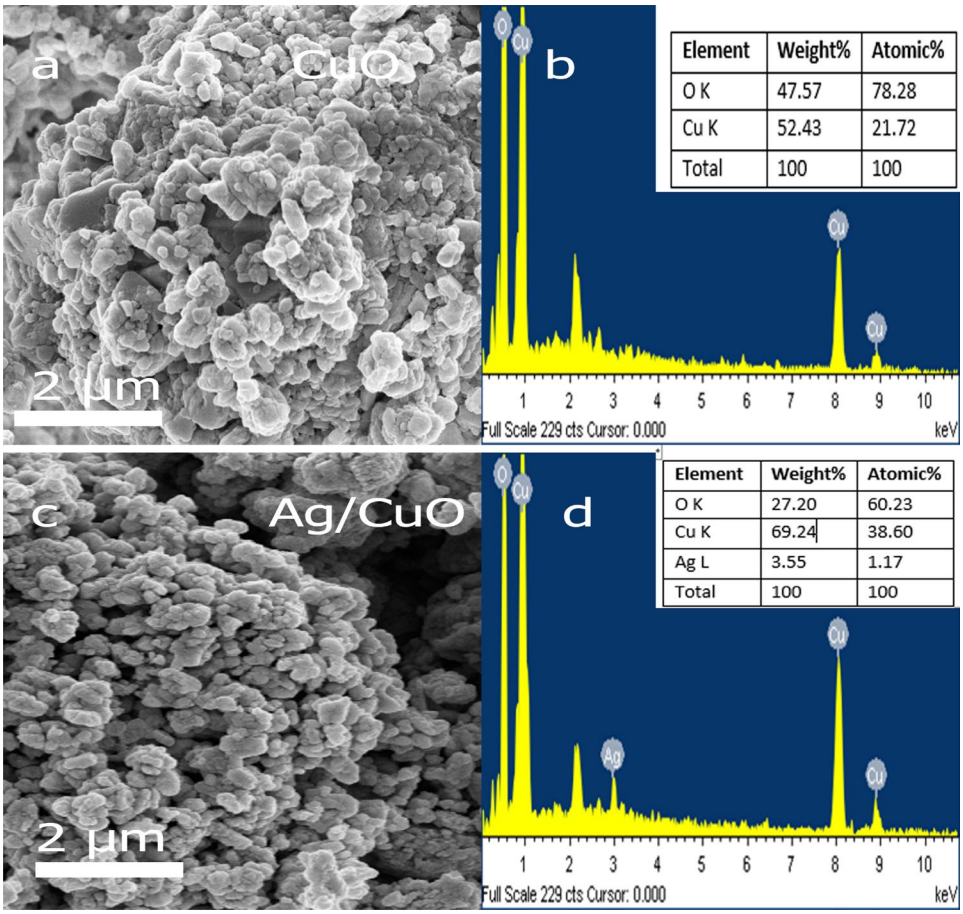

Fig. 4 SEM (**a** and **c**) and EDX (**b** and **d**) images of CuO and Ag/CuO NPs

XPS analysis

The chemical state and valency and binding energy are investigated by X-ray photoelectron spectroscopy (XPS) characterization. The optical application is based on the valence state of the NPs. Figure 7a–e shows the XPS spectrum of Ag/CuO NPs in wide, Ag, Cu, O, and C spectra, respectively. A wide spectrum (Fig. 7a) consists of core Ag metals, Cu2p, O1s, and C1s. The Ag $3d_{5/2}$ (366.6 eV) and Ag $3d_{5/2}$ (372.6 eV) peaks represent the metallic Ag core (Fig. 7b)with a difference of 6 eV in the spin–orbit coupling (Jesús Ruíz-Baltazar et al. 2018). The Cu 2p spectrum (Fig. 7(c)) indicates the four peaks of the copper state. The main peaks at Cu $2p_{3/2}$ (934.56 eV) and Cu $2p_{1/2}$ (954.56 eV) with a peak difference of 20 eV, which is well documented with a standard CuO spectrum (Sukumar et al. 2020). The other two copper peaks identify the existence of Cu^{2+} ions with the resemblance of the Cu_2O phase. The O1s spectrum (Fig. 7d) depicted the relationship between the Cu–O (531 eV). The lattice oxygen peaks confirm the binding with the Cu–O and Ag–Cu–O formation. The formation led by the *Cyperus pangorei* plant extract reduction, which is mainly reduced the Cu^{2+} and Ag^{+} ions and re-oriented with the lattice oxygen. The plant phytochemicals reduction was confirmed by C = O (534 eV) peak. The C1s (C–C = 283.6 eV, C–O = 285.2 eV, C = O 287.3 eV and C = O 287.5 eV) peak promotes the authenticity of the plant extract phytochemicals reaction with the Ag^{+} and Cu^{2+} existence (Li et al. 2020). The presence of Cu^{2+} in Cu $2p_{1/2}$ and Cu $2p_{3/2}$ is well bonded with the Ag ($3d_{5/2}$ and $3d_{3/2}$) and O. Hence the copper is more sensitive than silver for the oxidation process. The metal ions are surface bonded with lattice oxygen. Besides, the obtained results demonstrate the high purity Ag/CuO NPs. The oxidized metal NPs widely used the catalytic and optical, and energy applications. The obtained valency state has opted for the photocatalytic application.

Antibacterial activity

Antibacterial activity of biosynthesized CuO and Ag/CuO nanoparticles are shown in Fig. 8. The antibacterial activity against both bacteria *S. aureus* and *E. coli* increased with the increasing concentration of CuO and Ag/CuO from 5 to 20 µg/ml. Compared to CuO, the Ag/CuO NPs have exhibited an enhanced inhibition zone due to Ag presence on the surface of CuO nanoparticles (Table 1). In CuO nanoparticles, the 5 and 10 µg/ml showed no inhibition against *S.*

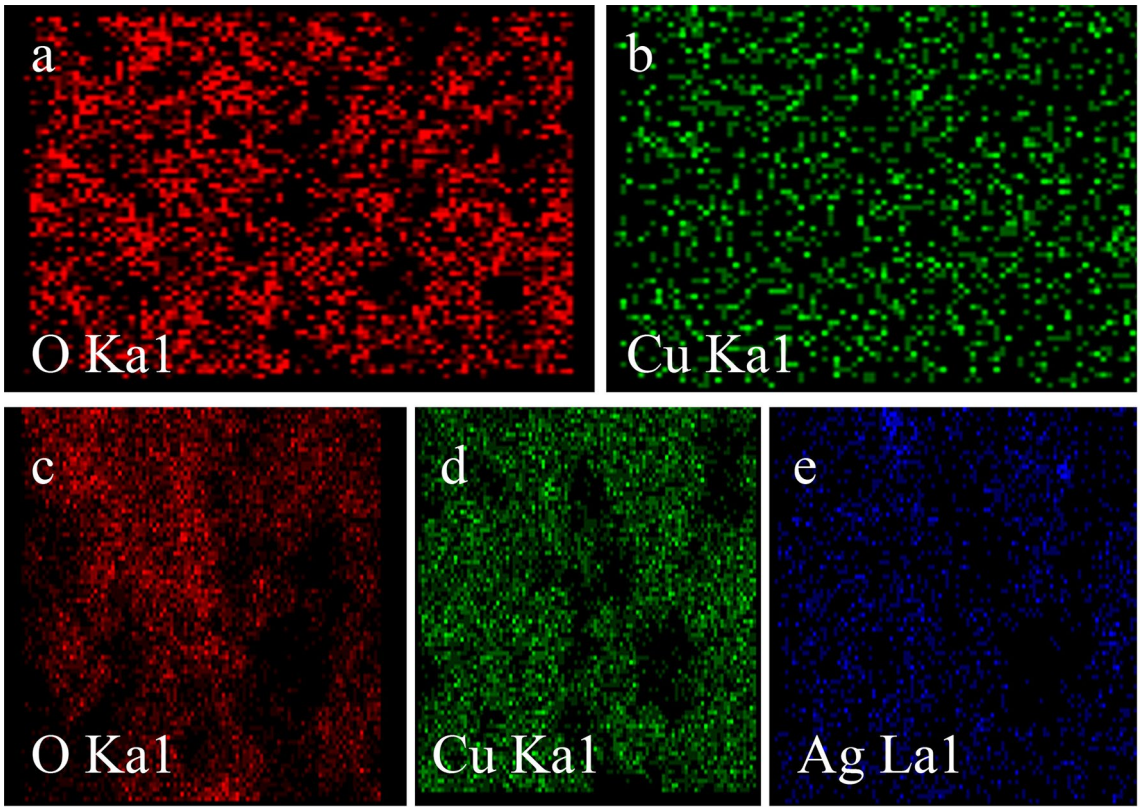

Fig. 5 Mapping images of CuO (**a** and **b**) and Ag/CuO NPs (**c**–**e**)

aureus reveals the bacteria is susceptible to those concentrations. However, the 15 and 20 µg/ml exhibited the potent activity on the growth of *S. aureus*. In *E. coli*, the 5 µg/ml represented no activity, whereas the rest of the concentrations 10, 15, and 20 µg/ml showed excellent growth inhibition activity. Concurrently, the Ag/CuO NPs exhibited fine antibacterial activity against both bacteria at all concentrations. In Ag/CuO NPs, the 20 µg/ml expressed increased and intense activity compared to other concentrations. The release of Ag^+ and Cu^+ metal ions from Ag/CuO NPs might be a potent source for bacterial growth inhibition.

Growth measurement analysis

The growth measurement analysis was carried out to examine bacterial growth inhibition when treated with CuO and Ag/CuO NPs at different concentrations are represented in Fig. 9. The growth measurement analysis was correlated well with the agar-plate method. The occurrence of 5 and 10 µg/ml CuO NPs' absorbance tails nearby the pure *S. aureus* (without CuO NPs) indicates the negative impact of CuO NPs. Whereas, the presence of 15 and 20 µg/ml absorbance tails underneath the 10 µg/ml reveals the CuO nanoparticles effectively inhibited the growth of *S. aureus*. In the case of CuO-treated *E. coli*, the appearance of absorbance tail adjacent to pure *E. coli* culture (without CuO) indicates that the growth of organisms was not inhibited by the CuO nanoparticles. However, the absorbance tails of 10, 15, and 20 µg/ml beneath the 5 µg/ml reveals the CuO NPs strongly inhibited the growth and survival of *E. coli*.

The combination of Ag/CuO NPs effectually controls the growth of *S. aureus* and *E. coli* at various concentrations. Compared to *S. aureus*, the growth of *E. coli* was affected mainly by the Ag/CuO nanoparticles. The absorbance tails of 5, 10, 15 and 20 µg/ml Ag/CuO NPs beneath the pure *S. aureus* cultures show the forcible inhibition of bacterial growth. Likely, the *E. coli* cultures were also strongly inhibited by the various concentrations of Ag/CuO NPs. The reason behind the potent inhibition of both *S. aureus* and *E. coli* cultures growth was mainly denoting the presence of Ag metal ions on the surface of CuO NPs.

Antibacterial activity mechanism

The interaction, entry, and binding of NPs with specific enzymes/proteins are prominent in the antibacterial activity. Numerous previous reports are exemplified

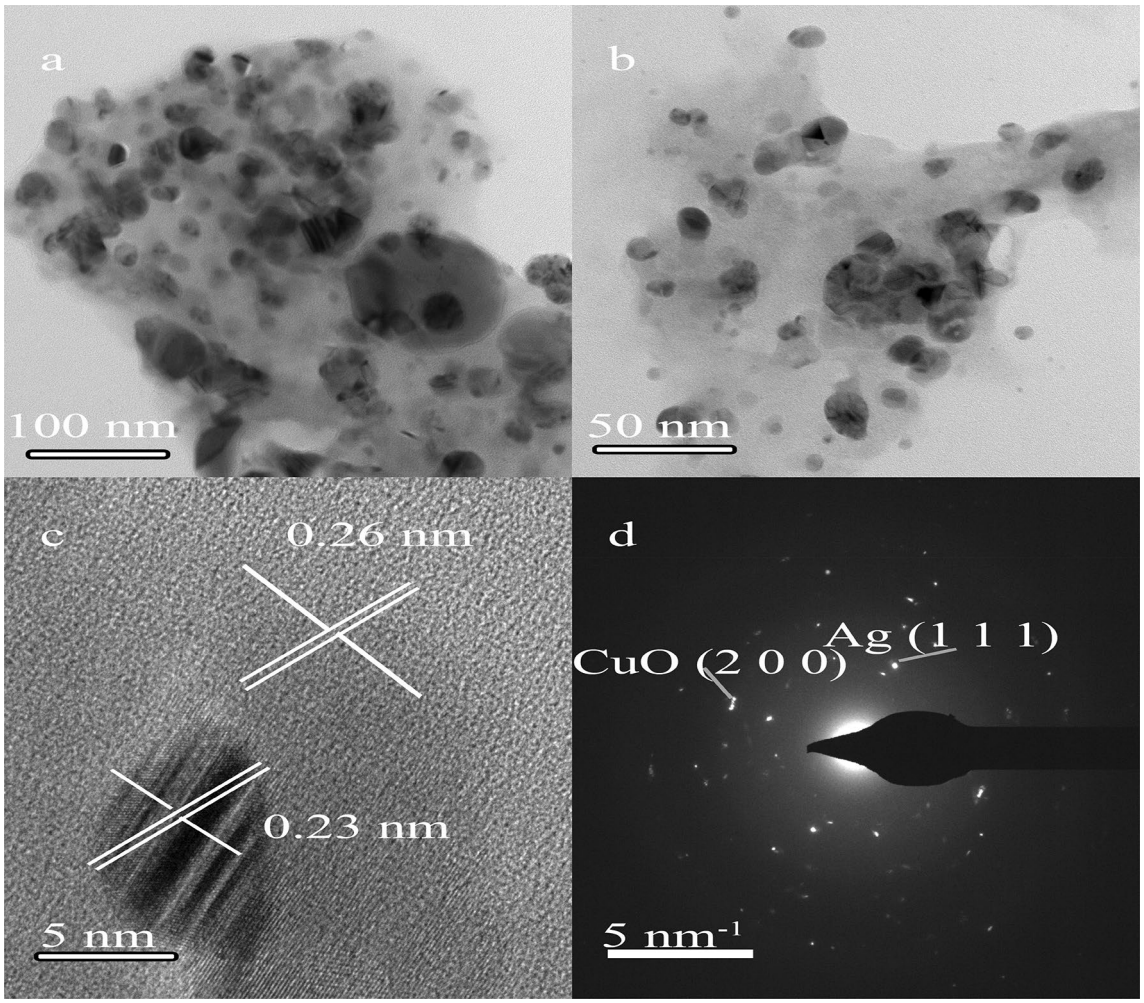

Fig. 6 TEM images of Ag/CuO NPs. **a** and **b** Different magnification, **c** lattice fringes, and **d** SAED pattern

the possible mechanism of antibacterial activity of NPs (Bandara et al. 2005; Wang et al. 2015; Kumar et al. 2014; Jyoti et al. 2016). Our present report also well concur with the previous literature statement. Prior, the release of Cu^{2+} ions from CuO NPs effectively binds with the negatively charged bacterial surface and collapse the organization of the membrane structural framework. Generally, we have known the Ag has remarkable potent antimicrobial activity against various microorganisms (Ouay and Stellacci 2015). Hence, the Ag^{+} ions with CuO NPs actively inhibit the growth of *S. aureus* and *E. coli*. The release of Ag^{+} and Cu^{2+} metal ions from CuO NPs may bind with the bacterial cell membrane by electrostatic interaction (Nabila and Kannabiran 2018; Jadhav et al. 2011; Li et al. 2010; Martínez-Castañon et al. 2008; Meghana et al. 2015) (Fig. 10). Further, they ruined the cell membrane structure and consequently, the release of cytoplasm may result in cell death. Moreover, Fig. 10 represents the Ag^{+} and Cu^{2+} metal ions dissolution can enhance the ROS formation and result in the inactivation of biomolecules, including DNA and proteins, which leads to cell death (Chen et al. 2019; Mousavi et al. 2020). Therefore, present antibacterial activity results suggested the combination of Ag^{+} with CuO NPs may be a nano-shield against various hazardous bacterial diseases.

Photocatalytic activity

The photocatalytic activity of biosynthesized CuO and Ag/CuO NPs were analyzed towards the degradation of Rh-B dye under visible light irradiation their spectrum results as shown in Fig. 11a, b. The Rh-B dye solution peak is 554 nm (without catalyst). The spectrum absorbance slowly decreasing using catalyst CuO and Ag/CuO

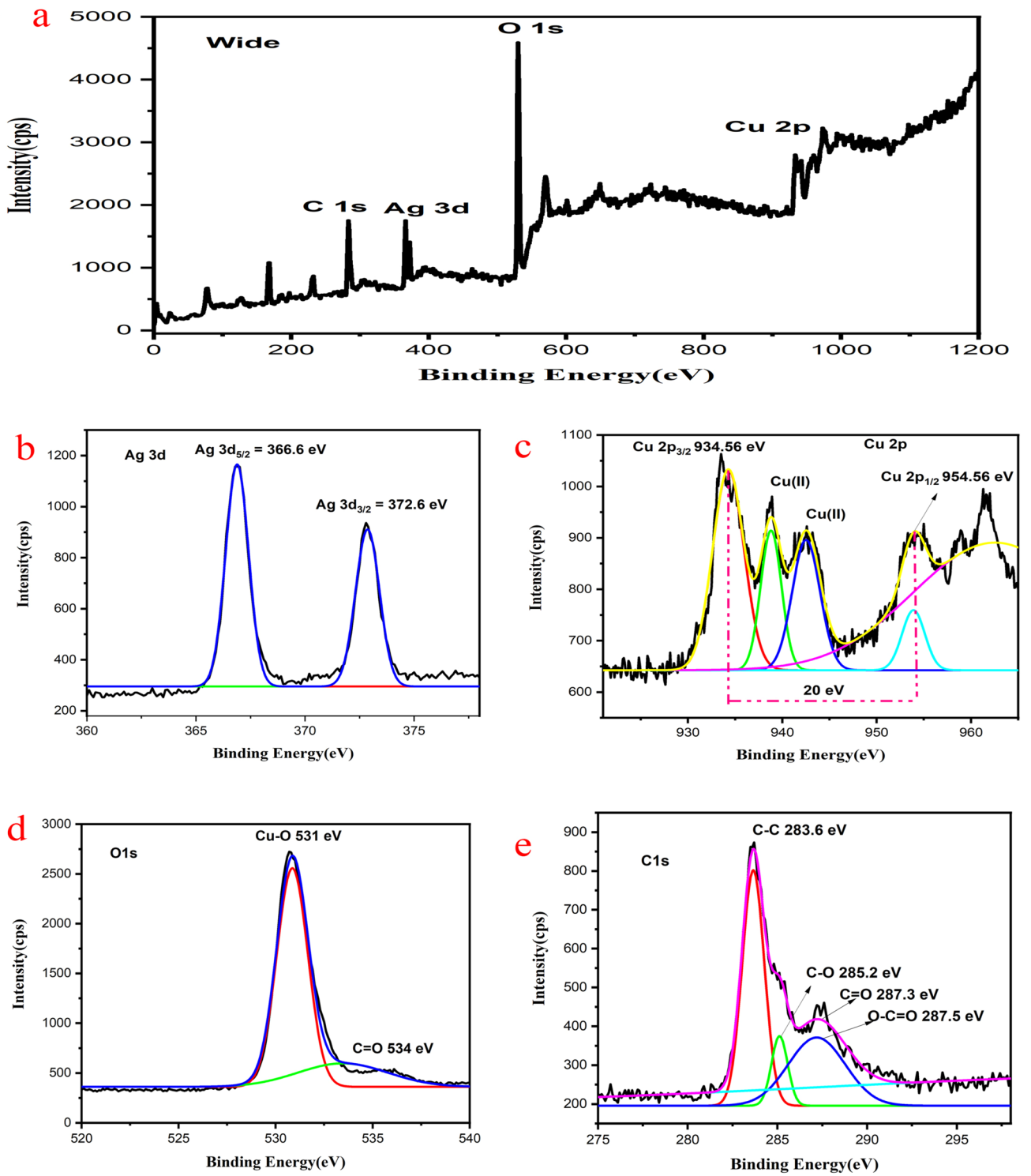

Fig. 7 XPS spectra of Ag/CuO NPs. **a** wide spectrum, **b** Ag 3d spectrum, **c** Cu 2p spectrum, and **d** O 1 s spectrum and **e** C 1 s spectrum

by depends on the time. The CuO NPs in the high catalytic activity of 120 min (74%) while the color dye solution slowly lost their colors with the time difference. The surface area of the copper oxides induces and improves the charge carriers for Rh-B in photocatalytic dye degradation (Shaabani et al. 2014). In Ag/CuO NPs having the photocatalytic activity of 120 min (92%). In the visible light irradiation (Xenon lamp) to the NPs, electrons

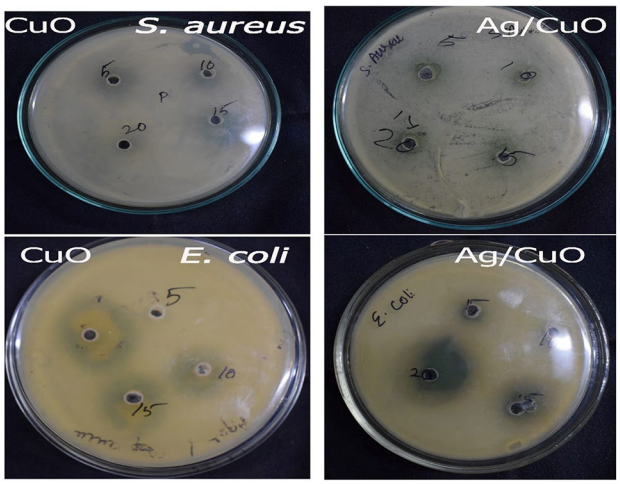

Fig. 8 Antibacterial activity of biosynthesized CuO and Ag/CuO nanoparticles

are easily excited from low energy valence band to high energy conduction band because of their low bandgap energy. During the process, electrons getting the property of reducing ability and holes getting the property of oxidation ability in the conduction band and valence band (Rao et al. 2020). The Ag cluster increases the gap of the copper oxide surface, which allows the light penetration to the sites whereas increasing the catalytic activity. Figure 11c represents Ag/CuO activity is higher than CuO of the photocatalytic activity. The surface plasmon resonance of the Ag is giving a large volume to surface area results in the improved dye degradation activity than CuO NPs. The detailed mechanism is shown in Fig. 11e and described as follows:

$$\mathrm{Ag/CuO} + hv \rightarrow e^{-}(\text{conduction band}) + h^{+}(\text{valence band}), \quad (3)$$

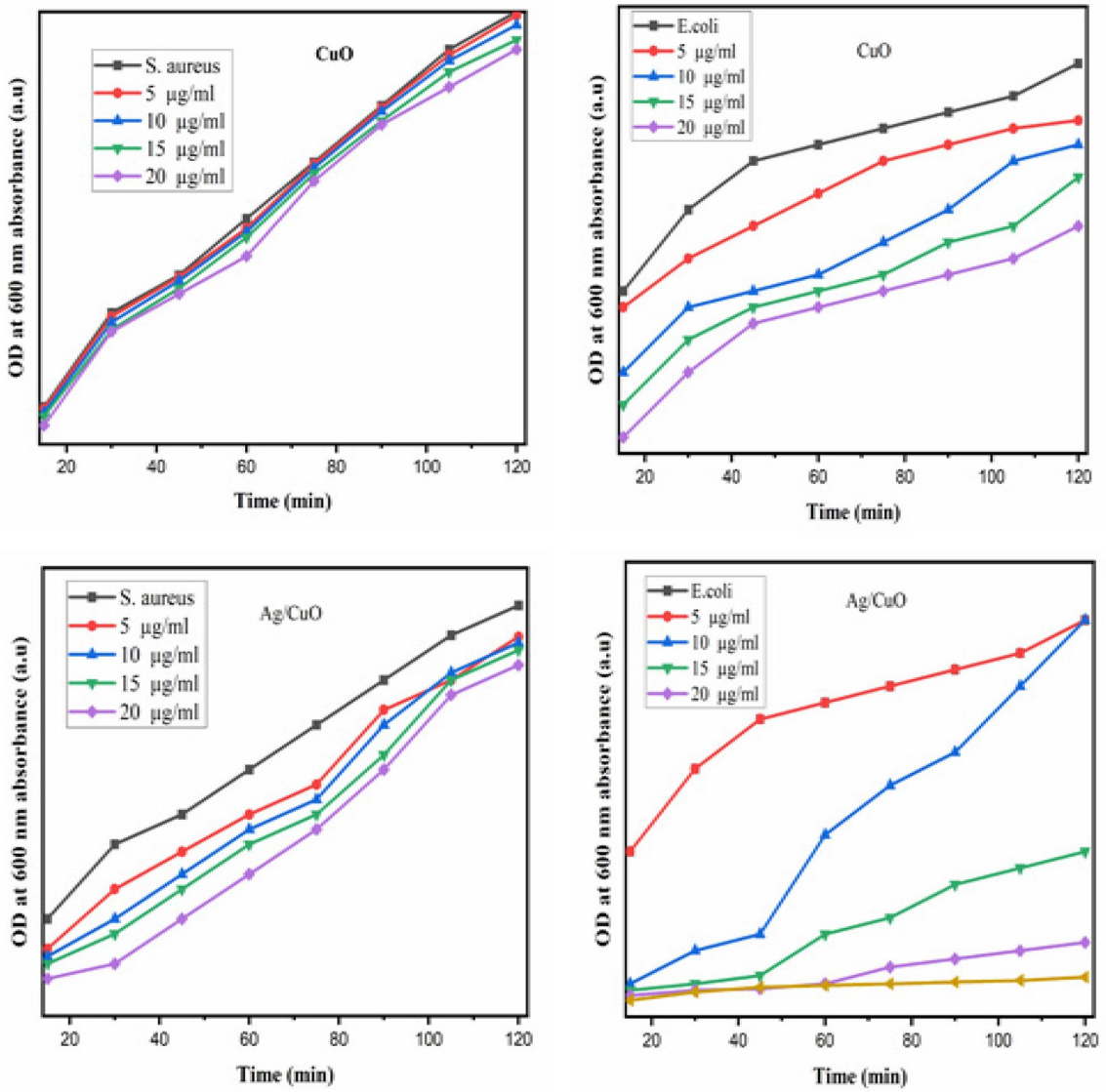

Fig. 9 Effect of bacterial growth *S. aureus* and *E. coli* in CuO and Ag/CuO nanoparticles

Table 1 Zone of inhibition of biosynthesized CuO and Ag/CuO nanoparticles in *S. aureus* and *E. coli*

Bacterial strain	CuO (µg/ml) in mm				Ag/CuO (µg/ml) in mm			
	5	10	15	20	5	10	15	20
S. aureus (+)	–	–	0.05	0.1	0.2	0.35	0.5	0.75
E. coli (−)	–	0.35	0.7	1.35	0.3	0.7	1.4	2.1

$$\left(H_2O \rightarrow H^+ + OH^-\right) + h^+(\text{valence band}) \rightarrow H^+ + OH, \quad (4)$$

$$O_2 + e^-(\text{conduction band}) \rightarrow O_2^- + H^+ + OH^- \rightarrow HO_2 + {}^-H, \quad (5)$$

$$HO_2 + {}^-OH + h^+(\text{valence band}) \rightarrow OH. \quad (6)$$

The excited electrons and holes possess a reduction and oxidation behavior. It has been suppressing the recombination of photoinduced electron–hole pair, which promotes the superoxides and free radicals formation. Three crucial parameters contribute to the photocatalytic activity,

(i) Illumination process implies the transition of electrons from valence band to the conduction band unoccupied sites of the holes. (ii) The excited energy (electrons and holes) can react to the catalytic exterior. (iii) Donors and acceptors are reacted with mutually to them.

The p-type semiconductor (CuO) produces the interior electric field, promoting the division of charge pairs and charges immigration. The electrons recombination frequently with the holes it has been break the energy in heat and light emission. The energy loss was sorting out by the AOP process. In Ag/CuO NPs banned by the recombination of electrons (Bharathi et al. 2020). The charge separation and immigration were controlled and induced by the interior electric field of Ag/CuO NPs. These processes provide the results of higher and better catalytic activity of Ag/CuO NPs. The photocatalytic dye degradation rate was calculated by pseudo-first-order kinetics, and it can be mentioned as follows (Kowalska et al. 2015):

$$-\ln\left(C_t/C_0\right) = -kt, \quad (7)$$

where C_t is the temporal concentration of Rh-B at time t, C_0 is the initial concentration of Rh-B, t is the degradation reaction time and k is the photocatalytic degradation rate constant. The rate constant is derived from the plotted graph is $-\ln(C_t/C_0)$ versus reaction time (t). The biosynthesized CuO and Ag/CuO NPs kinetics spectrum and values are shown in Fig. 11d.

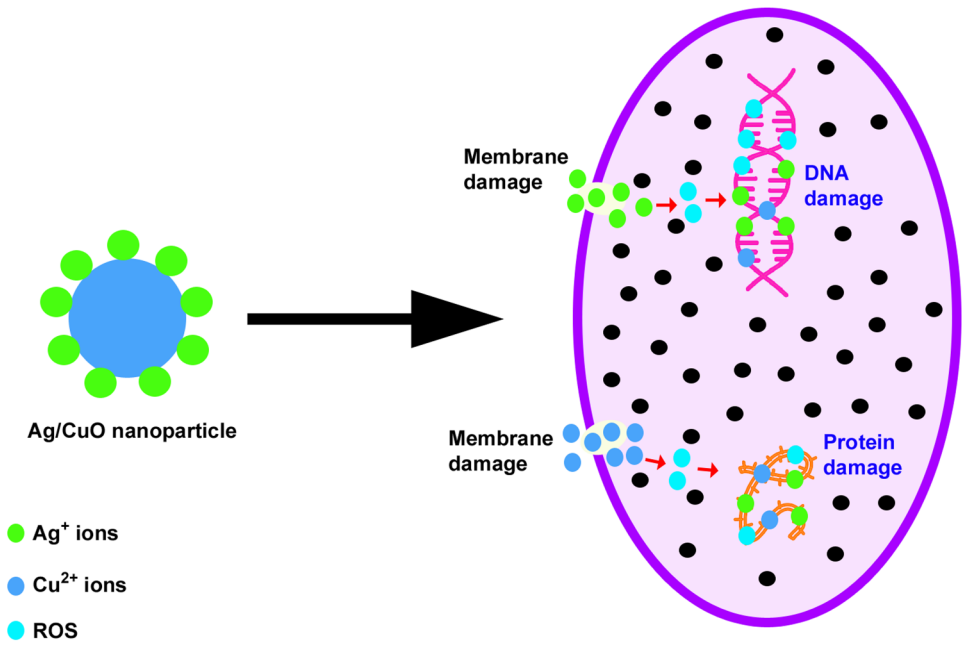

Fig. 10 Possible mechanism of antibacterial activity of Ag/CuO nanoparticles

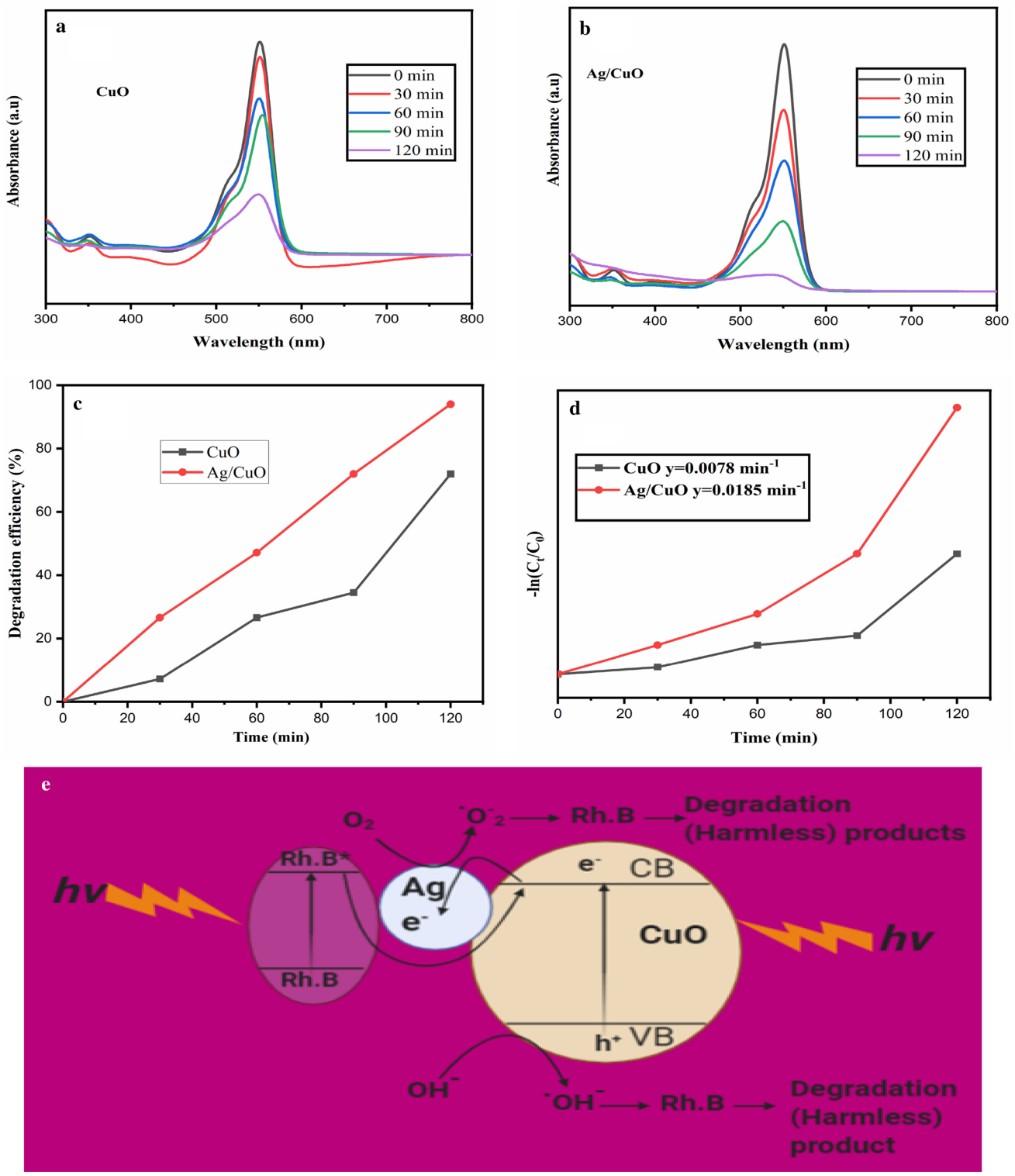

Fig. 11 Photocatalytic Rh-B dye degradation of CuO and Ag/CuO NPs. Degradation spectrum (**a**, **b**), degradation efficiency (**c**), pseudo-first-order kinetic (**d**), and mechanism (**e**)

Conclusion

The present study reports that the chemical-free *Cyperus pangorei* extract specified reduction. The structural and optical improvements confirmed the presence of Ag on the CuO surface. The monoclinic copper oxide character and the crystallized size increased because of their silver nanoparticles' surface modification. Surface modifications showed the SPR effect with a decrease in the bandgap. The presence of metallic silver on the surface of CuO increases the electron–hole pair life and improves the effective catalytic activity. The advanced oxidation method has modified and improved the energy separation of electrons. Consequently, no secondary contamination in the degradation process is more beneficial than other degradation processes. The results showed that CuO catalytic activity was inferior compared to Ag/CuO. Besides, the CuO and Ag/CuO expressed excellent antibacterial activity against both *S. aureus* and *E. coli*. The Ag/CuO NPs displayed their potent activity compared to the CuO NPs. Therefore, based on the present investigation findings, we have proposed that the biosynthesized CuO and Ag/CuO NPs are more efficient and higher potential wastewater treatment and nanomedicine applications.

Acknowledgements The authors would thank the facility of XRD, FTIR and UV–DRS, and research support given by the Department of Physics, Manonmaniam Sundaranar University, Tirunelveli. This research (SEM with EDX, TEM, and XPS) was performed using facilities at CeNSE, Indian Institute of Science, Bengaluru, funded by Ministry of Human Resource Development (MHRD), Ministry of Electronics and Information Technology (MeitY), and Nanomission, Department of Science and Technology (DST), Govt. of India.

Compliance with ethical standards

Conflict of interest There are no conflicts to declare.

References

Abrile MG, Fiasconaro ML, Lovato ME (2020) Optimization of Reactive Blue 19 dye removal using ozone and ozone/UV employing response surface methodology. SN Appl Sci 2:1–15

Bandara J, Udawatta CPK, Rajapakse CSK (2005) Highly stable CuO incorporated TiO_2 catalyst for photocatalytic hydrogen production from H_2O. Photochem Photobiol Sci 4(11):857–861

Baturay S, Tombak A, Kaya D, Ocak YS, Tokus M, Aydemir M, Kilicoglu T (2016) Modification of electrical and optical properties of CuO thin films by Ni doping. J Sol-Gel Sci Technol 78(2):422–429

Bharathi E, Sivakumari G, Kamalakkannan J, Karthikeyan B, Senthilvelan S (2020) Synergetic execute pressure, temperature on mixed Ac/Ag@ CuO and its multi properties of solar light elucidation and antibacterial activity by hydrothermal technique. Mater Sci Energy Technol 3:407–419

Chen J, Mao S, Xu Z, Ding W (2019) Various antibacterial mechanisms of biosynthesized copper oxide nanoparticles against soilborne *Ralstonia solanacearum*. RSC Adv 9(7):3788–3799

de Jesús Ruíz-Baltazar Á, Reyes-López SY, de Lourdes Mondragón-Sánchez M, Estevez M, Hernández-Martinez AR, Pérez R (2018) Biosynthesis of Ag nanoparticles using *Cynara cardunculus* leaf extract: evaluation of their antibacterial and electrochemical activity. Results Phys 11:1142–1149

El Shafey AM (2020) Green synthesis of metal and metal oxide nanoparticles from plant leaf extracts and their applications: a review. Green Process Synth 9(1):304–339

Farmer VC, Russell JD (1966) Effects of particle size and structure on the vibrational frequencies of layer silicates. Spectrochim Acta 22(3):389–398

Gunalan S, Sivaraj R, Venckatesh R (2012) Aloe barbadensis Miller mediated green synthesis of mono-disperse copper oxide nanoparticles: optical properties. Spectrochim Acta Part A Mol Biomol Spectrosc 97:1140–1144

Hariram M, Ganesan V, Muthuramkumar S, Vivekanandhan S (2021) Functionalization of kaolin clay with silver nanoparticles by Murraya Koenigii fruit extract-mediated bioreduction process for antimicrobial applications. J Aust Ceram Soc 1–9

He Q, Liang JJ, Chen LX, Chen SL, Zheng HL, Liu HX, Zhang HJ (2020) Removal of the environmental pollutant carbamazepine using molecular imprinted adsorbents: molecular simulation, adsorption properties, and mechanisms. Water Res 168:115164

Hemmati S, Mehrazin L, Hekmati M, Izadi M, Veisi H (2018) Biosynthesis of CuO nanoparticles using Rosa canina fruit extract as a recyclable and heterogeneous nanocatalyst for CN Ullmann coupling reactions. Mater Chem Phys 214:527–532

Jadhav S, Gaikwad S, Nimse M, Rajbhoj A (2011) Copper oxide nanoparticles: synthesis, characterization and their antibacterial activity. J Clust Sci 22(2):121–129

Jyoti K, Baunthiyal M, Singh A (2016) Characterization of silver nanoparticles synthesized using *Urtica dioica* Linn. leaves and their synergistic effects with antibiotics. J Radiat Res Appl Sci 9(3):217–227

Komeilibirjandi A, Raffiee AH, Maleki A, Nazari MA, Shadloo MS (2020) Thermal conductivity prediction of nanofluids containing CuO nanoparticles by using correlation and artificial neural network. J Therm Anal Calorim 139(4):2679–2689

Kowalska E, Wei Z, Karabiyik B, Herissan A, Janczarek M, Endo M, Ohtani B (2015) Silver-modified titania with enhanced photocatalytic and antimicrobial properties under UV and visible light irradiation. Catal Today 252:136–142

Kumar DA, Palanichamy V, Roopan SM (2014) Green synthesis of silver nanoparticles using *Alternanthera dentata* leaf extract at room temperature and their antimicrobial activity. Spectrochim Acta Part A Mol Biomol Spectrosc 127:168–171

Kumaravel V, Mathew S, Bartlett J, Pillai SC (2019) Photocatalytic hydrogen production using metal doped TiO_2: a review of recent advances. Appl Catal B 244:1021–1064

Le Ouay B, Stellacci F (2015) Antibacterial activity of silver nanoparticles: a surface science insight. Nano Today 10(3):339–354

Li WR, Xie XB, Shi QS, Zeng HY, You-Sheng OY, Chen YB (2010) Antibacterial activity and mechanism of silver nanoparticles on *Escherichia coli*. Appl Microbiol Biotechnol 85(4):1115–1122

Li H, Zou Y, Jiang J (2020) Synthesis of Ag@CuO nanohybrids and their photo-enhanced bactericidal effect through concerted Ag ion release and reactive oxygen species generation. Dalton Trans 49(27):9274–9281

Linke A, Weiss J, Kohlus R (2020) Oxidation rate of the non-encapsulated-and encapsulated oil and their contribution to the overall oxidation of microencapsulated fish oil particles. Food Res Int 127:108705

Liu C, Liu K, Wang C, Liu H, Wang H, Su H, Li X, Chen B, Jiang J (2020) Elucidating heterogeneous photocatalytic superiority of microporous porphyrin organic cage. Nat Commun 11(1):1–9

Martínez-Castañon GA, Nino-Martinez N, Martinez-Gutierrez F, Martinez-Mendoza JR, Ruiz F (2008) Synthesis and antibacterial activity of silver nanoparticles with different sizes. J Nanopart Res 10(8):1343–1348

Masudy-Panah S, Siavash Moakhar R, Chua CS, Kushwaha A, Dalapati GK (2017) Stable and efficient CuO based photocathode through oxygen-rich composition and Au–Pd nanostructure incorporation for solar-hydrogen production. ACS Appl Mater Interfaces 9(33):27596–27606

Meghana S, Kabra P, Chakraborty S, Padmavathy N (2015) Understanding the pathway of antibacterial activity of copper oxide nanoparticles. RSC Adv 5(16):12293–12299

Nabila MI, Kannabiran K (2018) Biosynthesis, characterization and antibacterial activity of copper oxide nanoparticles (CuO NPs) from actinomycetes. Biocatal Agric Biotechnol. https://doi.org/10.1016/j.bcab.2018.05.011

Mousavi SMAA, Mirhosseini SA, Panahi MRS, Hosseini HM (2020) Characterization of biosynthesized silver nanoparticles using lactobacillus rhamnosus GG and its in vitro assessment against colorectal cancer cells. Probiotics Antimicrob Proteins 12(2):740–746

Parvathiraja C, Shailajha S, Shanavas S, Gurung J (2020) Biosynthesis of silver nanoparticles by *Cyperus pangorei* and its potential in structural, optical and catalytic dye degradation. Appl Nanosci 11:1–15

Peng P, Huang H, Hu A, Gerlich AP, Zhou YN (2012) Functionalization of silver nanowire surfaces with copper oxide for surface-enhanced Raman spectroscopic bio-sensing. J Mater Chem 22(31):15495–15499

Picos-Corrales LA, Sarmiento-Sánchez JI, Ruelas-Leyva JP, Crini G, Hermosillo-Ochoa E, Gutierrez-Montes JA (2020) Environment-friendly approach toward the treatment of raw agricultural wastewater and river water via flocculation using chitosan and bean straw flour as bioflocculants. ACS Omega 5(8):3943–3951

Ranjith KS, Dong CL, Lu YR, Huang YC, Chen CL, Saravanan P, Asokan K, Rajendra Kumar RT (2018) Evolution of visible photocatalytic properties of Cu-doped CeO_2 nanoparticles: role of Cu^{2+}-mediated oxygen vacancies and the mixed-valence states of Ce ions. ACS Sustain Chem Eng 6(7):8536–8546

Rao MPC, Kulandaivelu K, Ponnusamy VK, Wu JJ, Sambandam A (2020) Surfactant-assisted synthesis of copper oxide nanorods for the enhanced photocatalytic degradation of reactive black 5 dye in wastewater. Environ Sci Pollut Res 27(15):17438–17445

Rasoulpour I, Jafarirad S (2017) Synthesis of biocapped CuO nanoparticles: an investigation on biorganic-Cu2+ interactions, in vitro antioxidant and antimicrobial aspects. Inorg Nano-Metal Chem 47(11):1599–1604

Raveesha HR, Sudhakar MS, Pratibha S, Ravikumara CR, Nagaswarupa HP, Dhananjaya N (2019) Costus Pictus leaf extract mediated biosynthesis of Fe and Mg doped CuO nanoparticles: structural, electrochemical and antibacterial analysis. Mater Res Express 6(11):1150.e5

Ruan D, Qin L, Chen R, Xu G, Su Z, Cheng J, Xie S, Cheng F, Ko F (2020) Transparent PAN: TiO_2 and PAN-co-PMA: TiO_2 nanofiber composite membranes with high efficiency in particulate matter pollutants filtration. Nanoscale Res Lett 15(1):1–8

Sankar R, Manikandan P, Malarvizhi V, Fathima T, Shivashangari KS, Ravikumar V (2014) Green synthesis of colloidal copper oxide nanoparticles using *Carica papaya* and its application in photocatalytic dye degradation. Spectrochim Acta Part A Mol Biomol Spectrosc 121:746–750

Scandelai APJ, Zotesso JP, Jegatheesan V, Cardozo-Filho L, Tavares CRG (2020) Intensification of supercritical water oxidation (ScWO) process for landfill leachate treatment through ion exchange with zeolite. Waste Manag 101:259–267

Shaabani B, Alizadeh-Gheshlaghi E, Azizian-Kalandaragh Y, Khodayari A (2014) Preparation of CuO nanopowders and their catalytic activity in photodegradation of Rhodamine-B. Adv Powder Technol 25(3):1043–1052

Sharifpour E, Alipanahpour Dil E, Asfaram A, Ghaedi M, Goudarzi A (2019) Optimizing adsorptive removal of malachite green and methyl orange dyes from simulated wastewater by Mn-doped CuO-Nanoparticles loaded on activated carbon using CCD-RSM: Mechanism, regeneration, isotherm, kinetic, and thermodynamic studies. Appl Organomet Chem 33(3):e4768

Singh R, Behera M, Kumar S (2020) Nano-bioremediation: an innovative remediation technology for treatment and management of contaminated sites. Bioremediation of industrial waste for environmental safety. Springer, Singapore, pp 165–182

Sukumar S, Rudrasenan A, Padmanabhan Nambiar D (2020) Green-synthesized rice-shaped copper oxide nanoparticles using caesalpinia bonducella seed extract and their applications. ACS Omega 5(2):1040–1051

Takasuga T, Takemori H, Yamamoto T, Higashino K, Sasaki Y, Weber R (2020) Comprehensive monitoring of chlorinated aromatic and heteroaromatic pollutants at sites contaminated by chlorine production processes to inform policy making. Emerg Contam 6:133–142

Tavares MG, Santos DH, Tavares MG, Duarte JL, Meili L, Pimentel WR, Zanta CL (2020) Removal of reactive dyes from aqueous solution by fenton reaction: kinetic study and phytotoxicity tests. Water Air Soil Pollut 231:1–15

Tunc I, Bruns M, Gliemann H, Grunze M, Koelsch P (2010) Bandgap determination and charge separation in $Ag@TiO_2$ core shell nanoparticle films. Surf Interface Anal 42(6–7):835–841

Wang LS, Deng JC, Yang F, Chen T (2008) Preparation and catalytic properties of Ag/CuO nano-composites via a new method. Mater Chem Phys 108(2–3):165–169

Wang Y, Zhang X, Liu J, Wang Y, Duan D, Fan C (2015) Facile regeneration and photocatalytic activity of CuO-modified silver bromide photocatalyst. Mater Sci Semicond Process 40:613–620

Wang X, Han Z, Liu Y, Wang Q (2020a) Micro-nano surface structure construction and hydrophobic modification to prepare efficient oil-water separation melamine formaldehyde foam. Appl Surf Sci 505:144577

Wang Y, Zhang Q, Li F, Gong J, Zhang X (2020b) Donor/acceptor maleimide and itaconimide dyes: synthesis, fluorescence and electrochemical properties. Dyes Pigm 172:107823

Xie W, Zhang Z, Liao L, Liu J, Su H, Wang S, Guo D (2020) Green chemical mechanical polishing of sapphire wafers using a novel slurry. Nanoscale 12(44):22518–22526

Yan Q, Wang XY, Feng JJ, Mei LP, Wang AJ (2020) Simple fabrication of bimetallic platinum-rhodium alloyed nano-multipods: a highly effective and recyclable catalyst for reduction of 4-nitrophenol and rhodamine B. J Colloid Interface Sci 582:701–710

Yu H, Cao C, Wang X, Yu J (2017) Ag-modified BiOCl single-crystal nanosheets: dependence of photocatalytic performance on the region-selective deposition of Ag nanoparticles. J Phys Chem C 121(24):13191–13201

Zhang Z, Song Y, Xu C, Guo D (2012a) A novel model for undeformed nanometer chips of soft-brittle HgCdTe films induced by ultrafine diamond grits. Scripta Mater 67(2):197–200

Zhang Z, Huo F, Zhang X, Guo D (2012b) Fabrication and size prediction of crystalline nanoparticles of silicon induced by nanogrinding with ultrafine diamond grits. Scripta Mater 67(7–8):657–660

Zhang Z, Huo Y, Guo D (2013) A model for nanogrinding based on direct evidence of ground chips of silicon wafers. Sci China Technol Sci 56(9):2099–2108

Zhang Z, Wang B, Kang R, Zhang B, Guo D (2015) Changes in surface layer of silicon wafers from diamond scratching. CIRP Ann 64(1):349–352

Zhang Z, Wang B, Zhou P, Kang R, Zhang B, Guo D (2016) A novel approach of chemical mechanical polishing for cadmium zinc telluride wafers. Sci Rep 6:26891

Zhang Z, Cui J, Wang B, Wang Z, Kang R, Guo D (2017a) A novel approach of mechanical chemical grinding. J Alloy Compd 726:514–524

Zhang Z, Huang S, Wang S, Wang B, Bai Q, Zhang B, Kang R, Guo D (2017b) A novel approach of high-performance grinding using developed diamond wheels. Int J Adv Manuf Technol 91(9–12):3315–3326

Zhang Z, Shi Z, Du Y, Yu Z, Guo L, Guo D (2018) A novel approach of chemical mechanical polishing for a titanium alloy using an environment-friendly slurry. Appl Surf Sci 427:409–415

Zhang Z, Cui J, Zhang J, Liu D, Yu Z, Guo D (2019) Environment friendly chemical mechanical polishing of copper. Appl Surf Sci 467:5–11

Zhang Z, Liao L, Wang X, Xie W, Guo D (2020a) Development of a novel chemical mechanical polishing slurry and its polishing mechanisms on a nickel alloy. Appl Surf Sci 506:144670

Zhang H, Gong W, Bai L, Chen R, Zeng W, Yan Z, Li G, Liang H (2020b) Aeration-induced CO_2 stripping, instead of high dissolved oxygen, have a negative impact on algae–bacteria symbiosis (ABS) system stability and wastewater treatment efficiency. Chem Eng J 382:122957

Zou Z, Wang Y, Huang J, Lei Z, Wan F, Dai Z, Yi L, Li J (2020) A study on the mixture repairing effect of biochar and nano iron oxide on toxicity of Cd toward muskmelon. Environ Pollut 266:115371